Published in final edited form as:

Mol Genet Metab. 2020 November ; 131(3): 306–315. doi:10.1016/j.ymgme.2020.09.005.

A novel *Pah*-exon1 deleted murine model of phenylalanine hydroxylase (PAH) deficiency

Daelyn Y. Richards[a], **Shelley R. Winn**[a], **Sandra Dudley**[a], **Lev Fedorov**[b], **Nicole Rimann**[c], **Beat Thöny**[c], **Cary O. Harding**[a,*]

[a]Department of Medical and Molecular Genetics, Oregon Health & Science University, Portland, USA [b]Transgenic Mouse Models Core, Oregon Health and Science University, Portland, USA [c]Division of Metabolism, University Children's Hospital, Steinweissstrasse 75, Zurich CH-8032, Switzerland

Abstract

Phenylalanine hydroxylase (PAH) deficiency, colloquially known as phenylketonuria (PKU), is among the most common inborn errors of metabolism and in the past decade has become a target for the development of novel therapeutics such as gene therapy. PAH deficient mouse models have been key to new treatment development, but all prior existing models natively express liver PAH polypeptide as inactive or partially active PAH monomers, which complicates the experimental assessment of protein expression following therapeutic gene, mRNA, protein, or cell transfer. The mutant PAH monomers are able to form hetero-tetramers with and inhibit the overall holoenzyme activity of wild type PAH monomers produced from a therapeutic vector. Preclinical therapeutic studies would benefit from a PKU model that completely lacks both PAH activity and protein expression in liver. In this study, we employed CRISPR/Cas9-mediated gene editing in fertilized mouse embryos to generate a novel mouse model that lacks exon 1 of the *Pah* gene. Mice that are homozygous for the *Pah* exon 1 deletion are viable, severely hyperphenylalaninemic, accurately replicate phenotypic features of untreated human classical PKU and lack any detectable liver PAH activity or protein. This model of classical PKU is ideal for further development of gene and cell biologics to treat PKU.

Keywords

Phenylketonuria; CRISPR/Cas9; Knockout mouse model; Gene therapy

*Corresponding author at: 3181 SW Sam Jackson Park Road, Mail Code L103, Portland, Oregon 97239, USA. hardingc@ohsu.edu (C.O. Harding).

Author contributions

D.R. performed the experiments, analyzed data, and wrote the manuscript.

L.F. assisted with experimental design and manuscript editing.

S.W. performed surgical procedures and assisted with experimental design, mouse breeding, molecular techniques, and editing of the manuscript.

S.D. assisted with mouse breeding and molecular techniques.

N.R. and B.T. performed the brain monoamine neurotransmitter analysis, and B.T. edited the manuscript.

C.H. assisted with funding, experimental design, analyses, data interpretation, manuscript editing, and was primary mentor to D.R. during graduate school.

Supplementary data to this article can be found online at https://doi.org/10.1016/j.ymgme.2020.09.005.

1. Introduction

Phenylketonuria (PKU) (OMIM # 261600) is among the most well-studied inborn errors of metabolism. PKU is most commonly caused by phenylalanine hydroxylase (PAH, EC 1.14.16.1) deficiency as the result of inherited *PAH* mutations, but can also be caused by mutations in the *DNAJC12* gene, one of the co-chaperones required for proper PAH folding and degradation [1]. PAH deficiency results in hyperphenylalaninemia (HPA) and irreversible neurological consequences if left untreated [2]. The PAH enzyme functions in liver as homo-tetramers to hydroxylate phenylalanine (Phe) into tyrosine and requires the co-factor tetrahydrobiopterin for catalysis [3]. Dietary phenylalanine (Phe) tolerance among PKU patients differs widely depending on the body's ability to maintain Phe homeostasis, resulting in a clinical continuum of phenotypes ranging from chronic mild hyperphenylalaninemia to severe classical PKU.

The *pah*$^{enu2/enu2}$ mouse model recapitulates classical PKU with toxic hyperphenylalaninemia that causes neurological damage if untreated, and due to this classical PKU phenotype, is the most utilized animal model for testing novel therapeutics. Elevated brain Phe impairs cognitive and behavioral performance, as well as proper monoamine neurotransmitter production [4]. Abundant stable, nonfunctional PAH protein that is recognized by anti-PAH antibodies is expressed in liver [5]. For research that aims to perform preclinical gene therapy studies, the presence of this mutant protein introduces confounding variables and challenges to experimental design, analysis, and interpretation. These challenges include the inability to distinguish transgene-derived functional enzyme from native mutant PAH by immunohistochemistry, as well as the dominant negative effect of mutant monomers forming hetero-tetramers with functional monomers, thereby lowering the overall activity of the holoenzyme complex [6]. In order to better evaluate genetic therapeutic interventions, a model that is completely void of PAH protein and activity is greatly desired. To accomplish this task, this study sought to delete the entire first exon of the *Pah* gene in C57BL/6 mouse embryos using the CRISPR/Cas9 system [7].

2. Materials & methods

2.1. Experimental design

2.1.1. Guide design and validation—Single guide RNAs (sgRNA) were designed using the online guide design tools CHOPCHOP and MIT Guide Design, using nucleotides 87,521,818–87,522,107 of the murine GRCm38.p4 C57BL/6 J chromosome 10 sequence, which contains the 5′ untranslated region (5′ UTR) through intervening sequence 1 (IVS 1) of the *Pah* locus. Of eight guides produced (Fig. 1A), six were selected for further sgRNA investigation (guides 1,3,4,6,7,8). All guides were tested with the Takara Guide-It sgRNA *In-Vitro* Transcription Kit (Cat. No. 632635) and Screening System (Cat. No. 632639). Guides 3, 4, 6, 7 and 8 proved effective at inducing a targeted double-stranded break in the PCR substrate, and only guide 1 was unable to induce a cut in the target DNA (Fig. 1B). The sgRNAs 4 and 8, located in the 5′ UTR and IVS1, respectively, were selected for *Pah* gene targeting in murine embryos (Fig. 1C).

2.1.2. Delivery of Cas9/sgRNA to mouse zygotes—Female C57BL/6N JAX® mice at 4–5 weeks of age were superovulated, mated with males, and 0.5 day old single cell zygotes were isolated as previously described [8]. Two approaches to accomplish mouse *Pah* exon 1 deletion were performed in this study. In the first approach, a mixture of Cas9 mRNA and sgRNAs were injected into the cytoplasm of the one-cell fertilized eggs [9]. In the second approach, electroporation of Cas9 protein/sgRNA (RNP) complex using the NEPA21 system (NEPA GENE Co. Ltd., Chiba Japan) was performed on single-cell fertilized eggs [10]. Zygotes from either approach were then transferred into the oviducts of pseudo pregnant recipient CD1/NCrl foster dams (Charles River), and the surviving offspring were screened for sizable deletions in the *Pah* exon 1 region after weaning.

2.1.3. PCR screen for deleted alleles—Tail biopsies were acquired from F0 animals at three weeks of age and screened for visually discernable deletions of 200 bp or more using standard PCR and gel electrophoresis. Forward primer 5′-GGTTGCGGAGAATCCATAC-3′ and reverse primer 5′-TGACTAAGGACCAGCCATTTC-3′ which are complementary to *Pah* sequences outside the putative Cas9 cleavage sites were used to amplify 753 bp spanning the 5′ UTR and 3′ IVS1 of exon 1 in the *Pah* locus using standard PCR with Invitrogen Platinum™ Taq DNA polymerase and the following cycling parameters: initial denaturation at 94 °C for 5 min, followed with 30 cycles of denaturation at 94 °C for 30 s, primer annealing at 55 °C for 30 s, and extension at 72 °C for 1 min, and a final extension of 72 °C for 5 min. Products were analyzed by electrophoresis on a 1% agarose gel with 1 kb NEB ladder (Fig. 1D and E). Bands approximately 500 bp in size were excised from the gel and purified with the Qiagen QIAQuick Gel Extraction kit (Cat. 28706 × 40) for Sanger sequencing.

2.1.4. Knockout-allele sanger sequencing—Purified approximately 500 bp PCR products described above were quantified using the Epoch Microplate Spectrophotometer and analyzed by standard Sanger sequencing with 5′-GGTTGCGGAGAATCCATAC-3′ forward primer on an ABI 3130XL sequencer.

2.2. Animal studies

2.2.1. Animal husbandry—Animal care and experimentation were performed in accordance with the guidelines of the Dept. of Comparative Medicine, Oregon Health & Science University and the National Institutes of Health Guide for the Care and Use of Laboratory animals. The knockout $Pah^{\Delta exon1/\Delta exon1}$ mice were produced through male $Pah^{+/\Delta exon1}$ x female $Pah^{+/\Delta exon1}$ as well as male $Pah^{\Delta exon1/\Delta exon1}$ x female $Pah^{+/\Delta exon1}$ crosses. Pups were toe clipped at two weeks for genotyping and identification purposes. All mice were fed tap water and standard mouse chow (LabDiet Picolab Rodent Diet 5LOD, St. Louis, MO) *ad libitum* providing approximately 24% protein and 1.04% *L*-phenylalanine by weight, except breeders that received high energy chow (LabDiet Rodent High Energy Diet 5058, St. Louis, MO) approximately 22% protein and 0.99% *L*-phenylalanine. Given that adult mice consume approximately 5 g chow per day, daily *L*-phenylalanine intake is estimated to be approximately 50 mg per day. The animals were housed under a standard 12 h on, 12 h off light cycle. All surgical procedures were carried out with inhaled isoflurane general anesthesia to minimize pain and discomfort.

2.2.2. Gene therapy—Three 6–8 week old *Pah*$^{\Delta exon1/\Delta exon1}$ mice (two males and one female) were treated with recombinant liver tropic adeno-associated virus serotype 8 vector containing AAV 2 genome (AAV2/8) that expressed the murine Pah cDNA from a strong Liver Specific Promoter (LSPmPAH) at doses of either 1×10^{10} vector genomes (vg) (1 male), 1×10^{11} vg (1 female), or 1×10^{12} vg (1 male) per mouse *via* retro-orbital injection. An additional control female animal was administered 1×10^{12} vg of a similar viral vector containing an inactivating frameshift mutation in the transgene, denoted as AAV2/8 LSPmPAHfs. Blood was obtained prior to AAV injection for measurement of blood Phe concentration. Two weeks later animals were harvested for molecular analyses, including serum and brain amino acid analysis, brain neurotransmitter analysis, hepatic PAH enzyme activity, liver PAH fluorescent-immunohistochemistry, and quantitative PCR (qPCR) to determine vg copy number in total liver DNA.

A similar gene therapy study was performed in the *pah*$^{enu2/enu2}$ mouse model. Two cohorts of six adult *pah*$^{enu2/enu2}$ animals (3 male and 3 female) were administered 1×10^{11} vg or 1×10^{12} vg AAV2/8 LSPmPAH *via* retro-orbital injection. Blood was obtained prior to AAV injection for measurement of blood Phe concentration. Two weeks later animals were harvested for molecular analyses, including serum Phe concentration, hepatic PAH enzyme activity, and quantitative PCR (qPCR) to determine vg copy number in total liver DNA.

2.2.3. Euthanasia and tissue harvest—Animals were sedated using inhaled isoflurane anesthesia. Whole blood was collected by cardiac puncture, allowed to clot in an Eppendorf tube, and serum was separated by centrifugation. The mice were then euthanized by exsanguination and perfused with 20 mL normal saline *via* the left cardiac ventricle to clear blood from the liver and brain.

2.3. Molecular characterization

2.3.1. Blood and brain amino acids—Blood and brain amino acid concentrations were determined using an established protocol [4] by pre-column derivatization with 6-aminoquinolyl-N-hydroxysuccinimidyl carbamate (AQC, Waters AccQ Tag™derivitization system) and separation by ultrahigh performance liquid chromatography and UV absorbance detection (Waters Acquity™ UPLC, Milford, MA) using the Waters Masstrak Amino Acid Analysis method (Fig. 2B and C).

2.3.2. Brain neurotransmitters—Mouse half brains were processed as previously described [4,11] for the measurement of dopamine, homovanillic acid (HVA), 5-hydroxytryptophan (5-HTP), serotonin, and 5-hydroxyindoleacetic acid (5-HIAA) through ultrahigh performance liquid chromatography (UHPLC) and electrochemical detection basically as previously established [12]. Neurotransmitter concentrations were corrected for the total protein content of brain homogenate and reported as nmol/g protein (Fig. 2D, E, F and G).

2.3.3. Liver PAH enzyme activity—PAH enzyme activity was determined in liver homogenates using a radiometric chromatography assay [13] with modifications [14],

corrected for protein content, and normalized to the measured wild type C57Bl/6 liver PAH activity from the same run (Fig. 3A).

2.3.4. Liver PAH Western blot—Bulk liver homogenates were prepared by mechanical homogenization of four 10 mg biopsies in 800 μL of cold lysis buffer, followed by centrifugation at 770 rpm for 8 min at 4 °C. The supernatant was collected and quantified for protein concentration using the Micro BCA™ Protein Assay Kit from ThermoFisher (Cat. 23,235). Each lane was loaded with a sample preparation containing 250 ng of protein in 1 μL, NuPage LDS Sample Buffer, 50 mM dithiothreitol, and water up to a total volume of 10 μL and incubated at 70 °C for 10 min. 3 μL of Magic Mark™ ladder and 10 μL of each sample were loaded on a NuPage precast gel and separated by electrophoresis in MOPS buffer at 200 V for 50 min. The protein was transferred to a polyvinylidene fluoride membrane with electrophoresis in NuPage transfer buffer at 100 V for 45 min. The membrane was blocked with 5% milk in TBS-T (Tris Buffer Saline-Tween) and probed with rabbit polyclonal anti-PAH antibody (1:200 dilution, BS3704 PAH (R400) from Bioworld, Inc.) and GAPDH loading control antibody (1:200 dilution, MA5-15738 GAPDH loading control antibody from Invitrogen) overnight. The membrane was washed with TBS-T and probed with HRP-conjugated goat anti-rabbit IgG secondary antibody (1:1000 dilution, A27034 Goat anti-rabbit IgG (H + L) from Thermo Scientific and m-IgGκ BP-HRP Sc 506,102 from Santa Cruz Biotechnology) for one hour and washed. Bands were visualized using enhanced chemiluminescence (Chemiluminescent Western Blot Detection from ThermoScientific) captured on the Azure Sapphire Biomolecular Imager chemiluminescence detection system (Fig. 3B).

2.3.5. Quantitative PCR for vector genome copy number in total liver DNA—Total liver genomic DNA from untreated *Pah*$^{\Delta exon1/\Delta exon1}$ mice was spiked with linearized LSPmPAH vector DNA and then sequentially diluted to produce a series of qPCR standards with final concentrations of 0.1 vector genome/diploid liver genome (vg/dg), 1 vg/dg, 3 vg/dg, 10 vg/dg, 30 vg/dg, 100 vg/dg, or 300 vg/dg. Total liver DNA isolated from gene therapy treated animals (three AAV2/8 LSPmPAH animals and one AAV2/8 LSPmPAHfs animal), as well as an untreated *Pah*$^{\Delta exon1/\Delta exon1}$ animal as a negative control, were subjected to qPCR, along with the standard series, using SYBR Select MM (Applied Biosystems), forward primer PAH7.125F, and reverse primer PAH10.12R, to produce fluorescently labelled PCR products. Amplification was carried out and analyzed on a Qiagen Rotor-Gene Q real-time thermocycler. The number of AAV vg/dg from gene therapy treated mice was then estimated by comparing the C_t values from the unknowns to a linear regression curve of C_t *vs*. vg/dg generated from the standard series (Table 1). Each standard sample was amplified in duplicate to generate the standard curve, while each unknown was amplified in triplicate with the mean vg/dg reported in Table 1.

2.3.6. Liver PAH fluorescent immunohistochemistry—Select animals of *Pah*$^{+/+}$ and *Pah*$^{\Delta exon1/\Delta exon1}$ genotype, as well as gene therapy treated *Pah*$^{\Delta exon1/\Delta exon1}$ animals, underwent saline-paraformaldehyde perfusion in preparation for liver fixation and immunohistochemistry (Fig. 3C and Fig. 4). Under deep isoflurane inhaled anesthesia, mice were perfused with 0.9% saline *via* cardiac infusion to clear the hepatic circulation of blood.

Excised biopsies from each liver lobule were then fixed for 24 h in fixation solution (4% paraformaldehyde in phosphate buffered saline) followed by immersion in 25% buffered sucrose for an additional 24 h. Tissues were embedded in optimal cutting temperature media, sliced into 15 μm sections, and mounted on glass slides. Sections were treated (following blocking) with rabbit polyclonal anti-PAH antibody (1:200 dilution, BS3704 PAH (R400) from Bioworld, Inc.) and incubated for 2 h at room temperature. After appropriate washes, sections were treated with Alexa 488-conjugated goat anti-rabbit IgG secondary antibody (1:150 dilution, A11008 Alexa Fluor 488 goat anti-rabbit IgG (H + L) from Invitrogen) and incubated for one hour at room temperature. After washing, cover slips were mounted with Vectashield mounting medium containing DAPI. Images were captured on a Nikon H550L fluorescence microscope.

2.3.7. PCR amplification and Sanger sequencing of potential CRISPR/Cas9 off target mutation sites—Possible sites of off-target sgRNA-Cas9 genotoxicity were selected for Sanger sequencing analysis using the *in silico* COSMID tool [15], which used the guide 4 and guide 8 target sequence to determine the top four off-target sites in the mouse reference genome (GRCm38) for each guide. Sanger sequencing was performed for each region with location, off-target sequence, COSMID score (where lower score indicates higher likelihood of sgRNA-Cas9 double strand break lesions) and Sanger sequencing chromatogram displayed in Supplemental Fig. 1.

3. Results

3.1. Experimental design

3.1.1. Guide validation—Using two *in silico* single guide RNA (sgRNA) design tools, CHOPCHOP and MIT Guide Design, *Streptococcus pyogenes* Cas9 appropriate guides throughout the *Pah* 5′ upstream untranslated region (5′ UTR), exon 1, and intron 1 (IVS1) were identified (Fig. 1A). Six sgRNAs (labelled guides 1, 3, 4, 6, 7 & 8) were selected to test for effective targeted double-stranded DNA breaks (DSB) (Fig. 1A). Using the Takara *In Vitro* Guide-It assay, sgRNAs 3, 4, 6, 7 & 8 were identified as being effective at inducing a DSB in mouse DNA, provided the remaining necessary gene editing components, in an *in vitro* setting (Fig. 1B). Guide 4 (5′ UTR) and guide 8 (IVS 1) were selected to knockout exon 1 of the *Pah* gene in murine embryos (Fig. 1C). After CRISPR/Cas9-mediated *Pah* gene targeting, the zygotes were transferred into oviducts of pseudopregnant females yielding eighty-five liveborn F0 progeny.

3.1.2. Pah exon1 deletion screen—DNA isolated from tail biopsies of 85 potentially genetically altered offspring were analyzed for large deletions. PCR amplification of a 753 bp fragment flanking exon 1 in the *Pah* locus was performed, followed by gel electrophoresis, and screening for the presence of visually discernable deletions spanning approximately 200 bp or more (Fig. 1D). CRISPR-modified alleles that contained small indels not visually detectable or large deletions greater in span than the amplicon and that would therefore not be amplified with this screening procedure were not further sought. Apparent heterozygous *Pah* exon 1 deletions were detected in four female pups using this screening procedure, but only two could be confirmed and analyzed upon Sanger

sequencing. The first animal carried a 243 bp deletion that was designated as allele a (Fig. 1C). Unfortunately, this deleted allele was unable to be propagated through breeding and therefore was not further characterized. Fortunately, a 258 bp deletion spanning exon 1 in a second founder animal, confirmed with Sanger sequencing and designated as allele b, was successfully propagated to an F1 generation and bred to homozygosity (Fig. 1C, D, E and F). Hereafter, we designate this mutant allele *Pah*$^{\Delta exon1}$, and mice that are homozygous for this deleted allele as *Pah*$^{\Delta exon1/\Delta exon1}$, heterozygous as *Pah*$^{+/\Delta exon1}$, and wild type as *Pah*$^{+/+}$.

3.2. Characterization of Pah$^{\Delta exon1/\Delta exon1}$ animals

3.2.1. Breeding of C57BL/6-Pah$^{\Delta exon1/\Delta exon1}$ mice—Four *Pah*$^{+/\Delta exon1}$ X *Pah*$^{+/\Delta exon1}$ crosses generated 23 pups with the following genotypes obtained at two weeks of life: 6 *Pah*$^{+/+}$, 12 *Pah*$^{+/\Delta exon1}$, and 5 *Pah*$^{\Delta exon1/\Delta exon1}$. This yield of genotypes is consistent with the 1:2:1 ratio expected from Mendelian inheritance of a recessive trait (Chi square = 0.36, df = 2, between the probability of 0.9–0.1, and thus the null hypothesis that there is no difference between the observed and expected ratios was not rejected). This result indicates that homozygosity for the *Pah*$^{\Delta exon1}$ allele is not associated with embryonic or neonatal lethality. However, beyond 2 weeks age, we have observed spontaneous demise in 10/17 of *Pah*$^{\Delta exon1/\Delta exon1}$ animals during the transition from nursing to dependence upon solid food. *Pah*$^{\Delta exon1/\Delta exon1}$ mice that survive beyond weaning exhibit coat color hypopigmentation on an unrestricted diet (Fig. 2A), a characteristic phenotype of mouse models of PKU that results from phenylalanine-mediated competitive inhibition of the melanin-synthesizing enzyme tyrosinase [16].

3.2.2. Serum and brain amino acid profiles—Serum and brain amino acid profiles were examined in adult (6–12 week old) *Pah*$^{\Delta exon1/\Delta exon1}$ (N = 6, 1 male and 5 female), *Pah*$^{+/\Delta exon1}$ (N = 3, 1 male and 2 female), and *Pah*$^{+/+}$ (N = 3, 1 male and 2 female) animals (Fig. 2B). Serum phenylalanine levels in *Pah*$^{\Delta exon1/\Delta exon1}$ mice averaged 2172 ± 275 μM (mean ± SD), consistent with severe PKU, and were significantly elevated in comparison to either *Pah*$^{+/\Delta exon1}$ (80 ± 14 μM) or *Pah*$^{+/+}$ (78 ± 12 μM) mice by one-way ANOVA (F (2,9) = 156.7, $P < 0.0001$). There was no difference of hyperphenylalaninemia between male and female *Pah*$^{\Delta exon1/\Delta exon1}$ animals in an unpaired t-test, with an average of 2364 μM in 3 male mice and 2248 μM in 7 female mice (p-value 0.7035). Serum tyrosine concentration was statistically different between genotypes by one-way ANOVA (F (2, 9) = 6.090, $P = 0.0213$) with *Pah*$^{\Delta exon1/\Delta exon1}$ (49 ± 13 μM) less than *Pah*$^{+/+}$ animals (75 ± 10 μM) but not significantly different from *Pah*$^{+/\Delta exon1}$ (62 ± 5 μM).

Brain homogenates were analyzed for Phe, as well as the amino acid neurotransmitter precursors for dopamine and serotonin, tyrosine and tryptophan, respectively (Fig. 2C). Brain Phe content was statistically elevated in *Pah*$^{\Delta exon1/\Delta exon1}$ mice (817 ± 90 nmol/g) in comparison to either *Pah*$^{+/\Delta exon1}$ (146 ± 19 nmol/g) or *Pah*$^{+/+}$ animals (114 ± 9 nmol/g) in a one-way ANOVA (F(2, 9) = 154.2, $P < 0.0001$). There were no statistical differences in brain tyrosine or tryptophan between the *Pah*$^{\Delta exon1}$ allele genotypes (Fig. 2C), with brain Tyr of 90 ± 14 nmol/g and brain Trp of 26 ± 4 nmol/g in *Pah*$^{\Delta exon1/\Delta exon1}$ These data are similar to published brain large neutral amino acid profiles in *pah*$^{enu2/enu2}$ mice (brain Phe 762 ± 17 nmol/g, brain Tyr 85 ± 15 nmol/g, and brain Trp 20 ± 3 nmol/g) [4].

3.2.3. Brain neurotransmitters—The content of the monoamine neurotransmitters dopamine, 5-hydroxytryptophan (5-HTP), serotonin, and their metabolites homovanillic acid (HVA) and 5-hydroxyindoleacetic acid (5-HIAA) were examined in adult *Pah*$^{\Delta exon1}$ animals. There are two parallel pathways that lead to the synthesis and metabolism of dopamine and serotonin. In dopaminergic neurons, tyrosine hydroxylase converts tyrosine into L-DOPA, which can then be converted into dopamine by L-amino acid decarboxylase (L-AAAD). After dopamine is secreted into the synapse, it can either be taken up by dopamine specific transporter (DAT) or metabolized into HVA. In *Pah*$^{\Delta exon1}$ animals, there was no difference in brain dopamine between *Pah*$^{\Delta exon1/\Delta exon1}$ animals (196.8 ± 38.78 nmol/g protein), *Pah*$^{+/\Delta exon1}$ animals (260.6 ± 102.4 nmol/g) and *Pah*$^{+/+}$ animals (234.3 ± 24.13 nmol/g protein) by one-way ANOVA (F (2,8) = 1.129, $P = 0.3700$), (Fig. 2D). Interestingly, there was an significant difference in brain HVA among the groups (F (2,8) = 9.349, $P = 0.0081$), but *post hoc* intergroup comparison revealed only an unexplained significant increase ($P = 0.016$) in brain HVA of *Pah*$^{+/\Delta exon1}$ animals (28.51 ± 3.74 nmol/g protein) in comparison to *Pah*$^{+/+}$ animals (19.04 ± 2.03 nmol/g) but no significant difference ($P = 0.9453$) between *Pah*$^{\Delta exon1/\Delta exon1}$ animals (18.36 ± 3.73 nmol/g) and wild type mice (Fig. 2E).

In the serotonergic neurons, tryptophan hydroxylase converts tryptophan into 5-HTP, which can then be converted by L-AAAD into serotonin. After serotonin is secreted into the synapse, it can either be taken up by serotonin reuptake transporters or metabolized into 5-HIAA. In contrast to dopamine, the brain serotonin content was significantly different among *Pah*$^{+/+}$, *Pah*$^{+/\Delta exon1}$, *Pah*$^{\Delta exon1/\Delta exon1}$ mice (one-way ANOVA F (2,8) = 91.20, $P < 0.0001$), (Fig. 2F). Brain serotonin content was significantly lower ($p = 0.0001$) in *Pah*$^{\Delta exon1/\Delta exon1}$ animals (47.30 ± 5.79 nmol/g protein) than in wild type animals (90.53 ± 3.10 nmol/g). Inexplicably, brain serotonin was somewhat increased ($P = 0.002$) in *Pah*$^{+/\Delta exon1}$ mice (122.1 ± 12.8 nmol/g) although we analyzed only 3 mice in this group. Similarly, the brain content of 5-HIAA, a marker of serotonin turnover, was significantly different among the genotypes by one-way ANOVA (F (2, 8) = 22.42, $P = 0.0005$), (Fig. 2G). Brain 5-HIAA was significantly decreased ($P = 0.0048$) in *Pah*$^{\Delta exon1/\Delta exon1}$ animals (18.95 ± 6.28 nmol/g protein) in comparison to *Pah*$^{+/+}$ animals (73.60 ± 10.11 nmol/ g protein). Brain 5-HIAA content was not significantly different ($P = 0.1629$) between wild type and *Pah*$^{+/\Delta exon1}$ animals (100.3 ± 32.24 nmol/g protein).

3.2.4. PAH enzyme activity—Liver PAH enzymatic activity was measured in homogenates from *Pah*$^{\Delta exon1/\Delta exon1}$ and *Pah*$^{+/\Delta exon1}$ mice and compared to that of the existing PKU model, *pah*$^{enu2/enu2}$ along with *Pah*$^{+/enu2}$ mice (Fig. 3A). Liver PAH enzyme activity is expressed as the percent of wild type C57BL/6 liver activity. As expected, PAH activity was undetectable in liver of either *Pah*$^{\Delta exon1/\Delta exon1}$ or *pah*$^{enu2/enu2}$ mice However, there was a surprising difference in the liver PAH activity measured in heterozygous *Pah*$^{+/\Delta exon1}$ (58 ± 7% wild type activity) and *Pah*$^{+/enu2}$ (29 ± 5% wild type activity) mice, with a $P < 0.0001$ *via* post-hoc intergroup comparison analysis with Tukey multiple comparisons test (Fig. 3A).

3.2.5. PAH protein expression—Western blot analysis of bulk liver homogenate revealed no visible band for anti-PAH staining at the expected 50 kDa size in

Pah$^{\Delta exon1/\Delta exon1}$ animals (Fig. 3B). There is a strong band for PAH in *Pah*$^{+/+}$ animals, and less intense but visible PAH bands in *Pah*$^{+/\Delta exon1}$ and *pah*$^{enu2/enu2}$ animals. Bands staining for GAPDH at 37 kDa reveal similar protein loading in all samples.

Liver fluorescent-immunohistochemistry using anti-PAH antibody conjugated to Alexa Fluor 488 (green) and nuclear staining with DAPI (blue), revealed strong PAH expression in *Pah*$^{+/+}$ mice but complete absence of visible PAH expression in *Pah*$^{\Delta exon1/\Delta exon1}$ animals (Fig. 3C).

3.2.6. PCR amplification and Sanger sequencing of potential CRISPR/Cas9 off target mutation sites—PCR amplification and Sanger sequencing of the top four predicted off target sites for Cas9-mediated double strand breaks associated with each of the guide RNA sequences used to produce the *Pah* exon 1 deletion detected no deleterious sequence differences (Supplemental Fig. 1).

3.3. Gene addition therapy in Pah$^{\Delta exon1/\Delta exon1}$ animals

3.3.1. Gene therapy—In order to demonstrate applicability of this model, liver tropic recombinant adeno-associated virus serotype 8 (rAAV8) containing the murine *Pah* (*mPAH*) cDNA (rAAV2/8 LSPmPAH) [17] was administered to three homozygous *Pah*$^{\Delta exon1}$ animals in a small preliminary dose escalation experiment. The highest, middle, and lowest doses (1×10^{12} vector genomes (vg), 1×10^{11} vg, and 1×10^{10} vg of rAAV2/8 LSPmPAH, respectively) were delivered systemically *via* retro-orbital injection. A control animal received rAAV2/8 vector containing a nonsense frameshift mutation that abolishes PAH expression (1×10^{12} vg rAAV2/8 LSPmPAHfs). The phenylalanine levels in the three treated animals showed substantial correction in blood (127 μM, 194 μM, and 235 μM, respectively) and brain (382 nmol/g, 135 nmol/g, and 325 nmol/g, respectively) 14 days post-administration at all three vector doses while the animal that received the frameshift virus maintained elevated blood (1928 μM) and brain (1222 nmol/g) Phe levels (Table 1). Interestingly, the gene therapy treated animals exhibited liver PAH enzyme activity (96.1%, 42.0%, and 4.8% of wild type C57BL/6 liver activity), rAAV2 vector genome copy number (49.7 ± 2.9 vg, 16.2 ± 3.1 vg, and 2.9 ± 0.2 vg/ diploid liver genome), and intensity of liver fluorescent-immunohistochemical PAH staining that correlated with the vector dose (Table 1 and Fig. 4).

Similar gene addition therapy was administered to *pah*$^{enu2/enu2}$ animals (3 males and 3 females per dose) systemically through the retro-orbital route with doses of 1×10^{11} vg and 1×10^{12} vg of rAAV2/8 LSPmPAH, that conferred reduced Phe of 176 ± 52 μM and 99 ± 22 μM, respectively, % WT PAH enzyme activity of 7.7 ± 2.2% and 14.8 ± 3.3%, respectively, and vg/dg of 8–42 vg/dg and 56–291 vg/dg, respectively (Table 1).

4. Discussion

This study was able to successfully generate a novel murine model for classical PKU completely void of hepatic PAH protein expression. *Pah*$^{+/\Delta exon1}$ x *Pah*$^{+/\Delta exon1}$ mating produced the expected 1:2:1 Mendelian ratios of *Pah*$^{+/+}$ to *Pah*$^{+/\Delta exon1}$ to *Pah*$^{\Delta exon1/\Delta exon1}$ offspring. Additionally, female *Pah*$^{+/\Delta exon1}$ x male *Pah*$^{\Delta exon1/\Delta exon1}$ mating was productive,

yielding progeny in a 1:1 ratio of *Pah*$^{+/\Delta exon1}$ to *Pah*$^{\Delta exon1/\Delta exon1}$ animals Complete PAH deficiency did not cause embryonic or neonatal lethality. However, *Pah*$^{\Delta exon1/\Delta exon1}$ mice struggled to wean from nursing to solid food more frequently than the prior existing *pah*$^{enu2/enu2}$ model, with increased mortality at weaning. They required more attention to husbandry at this period with delayed separation from their dam and provision of soft food placed directly in the bottom of the cage until they demonstrated consistent ability to reach the chow overhead in the cage lid. The precise reason for this difference in the phenotype at weaning between the *Pah*$^{\Delta exon1/\Delta exon1}$ and *pah*$^{enu2/enu2}$ models requires further investigation. There were no other obvious differences in the physical phenotype or neurologic performance of the two models to explain the loss of *Pah*$^{\Delta exon1/\Delta exon1}$ mice near weaning. Blood and brain amino acid concentrations including the levels of phenylalanine and tyrosine in adult mice that survived weaning did not differ significantly between the two mouse strains, with the exception that the effect of sex upon serum Phe seen in *pah*$^{enu2/enu2}$ mice (higher mean blood Phe in females than in males) was not demonstrated in *Pah*$^{\Delta exon1/\Delta exon1}$ mice. Brain neurotransmitter evaluation in *Pah*$^{\Delta exon1/\Delta exon1}$ mice revealed findings analogous to those previously reported in the *pah*$^{enu2/enu2}$ model, which showed minimal disruptions in the dopamine pathway, but significant deficiencies in serotonin production [4]. The main biochemical difference between the *Pah*$^{\Delta exon1/\Delta exon1}$ and *pah*$^{enu2/enu2}$ models is the complete lack of detectable PAH protein in the knockout mouse. Deleterious CRISPR/Cas9-mediated mutation at an off-target site is a theoretical, low probability event that could adversely affect the phenotype of *Pah*$^{\Delta exon1/\Delta exon1}$ mice. PCR amplification and Sanger sequencing of the top four predicted off-target Cas9 cutting sites for each the two guides used to develop the mouse detected no genotoxicity at any of those eight locations, however this approach was not comprehensive for the entire genome. To eliminate the possibility of any adverse mutations at alleles other than *Pah*, we are currently outbreeding the *Pah*$^{\Delta exon1}$ allele onto a clean C57BL/6 genetic background.

Prior to this, the available mammalian animal models of PKU consisted of mouse models denoted as *Pah*$^{enu1/enu1}$, *pah*$^{enu2/enu2}$, and *Pah*$^{enu3/enu3}$, which were created by random N-ethyl-N-nitrosourea (ENU) mutagenesis [5]. The *Pah*^{enu3} allele, which is no longer available due to breeding difficulties and neonatal fatality, contained a frameshift mutation that caused premature termination of the tetramerization domain [18]. *Pah*^{enu1} and *Pah*^{enu2} alleles are missense mutations that result in phenotypes on opposite ends of the hyperphenylalaninemia spectrum and are the predominant models of PKU to date. An additional model of PKU combines *enu1* and *enu2* as a heteroallelic *Pah*$^{enu1/enu2}$ model, recapitulating compound heterozygosity for *PAH* mutations which occurs in approximately 87% of humans with PKU [19,20]. The *Pah*$^{\Delta exon1/\Delta exon1}$ and *Pah*$^{enu1/enu2}$ models are less desirable for gene and cell interventions due to their mild phenotype.

The longstanding and most popular mouse model for preclinical PKU gene therapy studies has been the *pah*$^{enu2/enu2}$ model, which is homozygous for a p.F263S (c.835 T > C) missense mutation in the central catalytic domain of PAH. It produces abundant albeit inactive PAH enzyme and recapitulates classical human PKU, with severe hyperphenylalaninemia, cognitive and behavioral disabilities, hypopigmentation, and occasional seizures. We and other groups have successfully treated adult *pah*$^{enu2/enu2}$ animals with AAV-mediated gene addition therapy demonstrating robust, long-term efficacy

[17,21-23]. Additionally, this model has been used in hepatocyte transplant studies [24-26] and CRISPR/Cas9-mediated gene correction of the *enu2* point mutation in neonatal [27] and adult animals [28]. While these studies have driven the advancements in PKU therapeutic development, there is a significant limitation in this model, specifically the expression of inactive PAH monomer, leading to barriers in both efficacy and molecular analyses of gene and cell therapeutic interventions. The expression of mutant PAH protein makes immuno-based molecular analyses using anti-PAH antibodies following gene therapy uninformative as the ability to quantify or localize transgene-delivered protein is limited. Additionally, it has been proposed that the native mutant PAH monomers interact with and reduce overall activity of wild type monomers, and in this mouse model, pose an additional barrier to efficacy in gene therapy studies.

The possibility that mutant PAH monomers might have a dominant negative effect upon the activity of wild type PAH was first suggested from a study of liver PAH activities measured in parents of children with PKU [29]. In these individuals who were presumably heterozygous for pathogenic *PAH* mutations (the study occurred prior to cloning of the *PAH* gene), liver PAH activity measured only 4.4–23% of wild type activity rather than the 50% typically expected for a recessively-inherited disorder. In this new study, we now confirm significant differences in liver PAH enzyme activity between $Pah^{+/\Delta exon1}$ and $Pah^{+/enu2}$ heterozygous animals, indicating that the production of mutant F263S monomers in $Pah^{+/enu2}$ heterozygous mice adversely impacted the proper function of wild type PAH. These data provide strong *in vivo* evidence for the dominant negative effect of at least this single missense *Pah* mutation. Further studies are warranted to confirm these findings and extend them to the Pah^{enu1} model. We propose that this phenomenon may extend to multiple human missense *PAH* mutations.

Preliminary results from a small liver-directed AAV8-mediated dose escalation gene addition trial in three $Pah^{\Delta exon1/\Delta exon1}$ mice revealed the utility of this model for liver gene transfer studies particularly in regard to employing anti-PAH immunohistochemistry in the assessment of hepatocyte transduction frequency, a feat that was previously unachievable in existing murine models. Furthermore, comparison of the efficacy in this small trial to the efficacy of $pah^{enu2/enu2}$ mice corroborates the suspicion that F263S mutant monomers present in the latter model inhibit the activity of wild type transgene-produced PAH and thereby limit treatment efficacy. Despite similar vector genome numbers within hepatocytes of the $Pah^{\Delta exon1/\Delta exon1}$ and $pah^{enu2/enu2}$ animals, PAH enzyme activity was far greater in the $Pah^{\Delta exon1/\Delta exon1}$ animals (Fig. 3A). More $Pah^{\Delta exon1/\Delta exon1}$ animals need to be treated to confirm these findings, but nevertheless we are confident in reporting that this knockout model is more sensitive to therapeutic intervention and is better able to depict a more accurate analysis of vector genome to PAH activity due to the lack of mutant monomer expression, ameliorating the dominant negative effect observed in $pah^{enu2/enu2}$ mice.

In conclusion, we report the development of a novel PAH deficient murine model harboring a recessively inherited deletion of *Pah* exon 1. Because anti-PAH immunohistochemistry can be readily employed to track hepatocyte transduction following gene therapy, in addition to an apparently improved therapeutic threshold in comparison to the existing Pah^{enn2} model, we predict that this novel model will find particular utility in the future investigation of gene

addition and gene editing methods. Importantly, with AAV-mediated gene addition therapy for PKU now entering human trials, this model provides a platform to more clearly correlate gene therapy treatment with physiological outcomes and aid our understanding of clinical trial results. While creating a model for classical PKU gene therapy with fewer confounding variables and enhanced molecular analyses was the impetus for this project, the overarching goal of generating this model was to add to the experimental tools available for PKU scientists and to advance PKU research.

Supplementary Material

Refer to Web version on PubMed Central for supplementary material.

Acknowledgements

We gratefully acknowledge Division of Comparative Medicine for mouse colony maintenance and Transgenic Mouse Models Shared Resource of OHSU for the generation of *Pah* mutant mice. We thank the DNA core facility of Vollum Institute at OHSU for sequencing analysis. We thank Anahita Rossi for technical assistance with the neurotransmitter measurements.

DYR and the experiments were funded by the National PKU Alliance, United States. SRW, SD, NR, BT, and COH were funded by NIH, USA, National Institute of Neurological Disorders and StrokeRO1 NS080866.

We would like to express our sincerest gratitude to the National PKU Alliance for supporting this research.

References

[1]. Jung-Kc K, et al., Phenylalanine hydroxylase variants interact with the co-chaperone DNAJC12, Hum. Mutat 40 (4) (2019) 483–494. [PubMed: 30667134]

[2]. Blau N, Genetics of phenylketonuria: Then and now, Hum. Mutat 37 (6) (2016) 508–515. [PubMed: 26919687]

[3]. Flydal MI, Martinez A, Phenylalanine hydroxylase: Function, structure, and reg-ulation, IUBMB Life 65 (4) (2013) 341–349. [PubMed: 23457044]

[4]. Winn SR, et al., Blood phenylalanine reduction corrects CNS dopamine and serotonin deficiencies and partially improves behavioral performance in adult phenylketonuric mice, Mol. Genet. Metab 123 (1) (2018) 6–20. [PubMed: 29331172]

[5]. Shedlovsky A, et al., Mouse models of human phenylketonuria, Genetics 134 (4) (1993) 1205–1210. [PubMed: 8375656]

[6]. Waters PJ, Scriver CR, Parniak MA, Homomeric and heteromeric interactions between wild-type and mutant phenylalanine hydroxylase subunits: Evaluation of two-hybrid approaches for functional analysis of mutations causing hyperphenylalaninemia, Mol. Genet. Metab 73 (3) (2001) 230–238. [PubMed: 11461190]

[7]. Doudna JA, Charpentier E, Genome editing. The new frontier of genome engineering with CRISPR-Cas9, Science 346 (6213) (2014) 1258096. [PubMed: 25430774]

[8]. Hogan BBR, Beddington R, Costantini F, Lacy E, Recovery, culture, and transfer of embryos and germ cells, Manipulating the Mouse Embryo: A Laboratory Manual, Cold Spring Harbor Press, 1994, pp. 127–188.

[9]. Qin W, et al., Generating mouse models using CRISPR-Cas9-mediated genome editing, Curr. Protoc. Mouse Biol 6 (1) (2016) 39–66. [PubMed: 26928663]

[10]. Remy S, et al., Generation of gene-edited rats by delivery of CRISPR/Cas9 protein and donor DNA into intact zygotes using electroporation, Sci. Rep 7 (1) (2017) 16554. [PubMed: 29185448]

[11]. Elzaouk L, et al., Dwarfism and low insulin-like growth factor-1 due to dopamine depletion in Pts −/− mice rescued by feeding neurotransmitter precursors and H4-biopterin, J. Biol. Chem 278 (30) (2003) 28303–28311. [PubMed: 12734191]

[12]. Blau N, et al., Variant of dihydropteridine reductase deficiency without hyper-phenylalaninaemia: Effect of oral phenylalanine loading, J. Inherit. Metab. Dis 22 (3) (1999) 216–220. [PubMed: 10384371]

[13]. Ledley FD, Hahn T, Woo SL, Selection for phenylalanine hydroxylase activity in cells transformed with recombinant retroviruses, Somat. Cell Mol. Genet 13 (2) (1987) 145–154. [PubMed: 3470952]

[14]. Harding CO, et al., Metabolic engineering as therapy for inborn errors of metabolism–development of mice with phenylalanine hydroxylase expression in muscle, Gene Ther. 5 (5) (1998) 677–683. [PubMed: 9797873]

[15]. Cradick TJ, et al., COSMID: A web-based tool for identifying and validating CRISPR/Cas off-target sites, Mol. Ther. Nucleic Acids 3 (2014) e214. [PubMed: 25462530]

[16]. Fitzpatrick TB, Miyamoto M, Competitive inhibition of mammalian tyrosinase by phenylalanine and its relationship to hair pigmentation in phenylketonuria, Nature 179 (4552) (1957) 199–200.

[17]. Harding CO, et al., Complete correction of hyperphenylalaninemia following liver-directed, recombinant AAV2/8 vector-mediated gene therapy in murine phenylketonuria, Gene Ther. 13 (5) (2006) 457–462. [PubMed: 16319949]

[18]. Haefele MJ, White G, McDonald JD, Characterization of the mouse phenylalanine hydroxylase mutation Pah(enu3), Mol. Genet. Metab 72 (1) (2001) 27–30. [PubMed: 11161825]

[19]. Sarkissian CN, et al., A heteroallelic mutant mouse model: A new orthologue for human hyperphenylalaninemia, Mol. Genet. Metab 69 (3) (2000) 188–194. [PubMed: 10767173]

[20]. Zurfluh MR, et al., Molecular genetics of tetrahydrobiopterin-responsive phenylalanine hydroxylase deficiency, Hum. Mutat 29 (1) (2008) 167–175. [PubMed: 17935162]

[21]. Ding Z, et al., Correction of murine PKU following AAV-mediated intramuscular expression of a complete phenylalanine hydroxylating system, Mol. Ther 16 (4) (2008) 673–681. [PubMed: 18362925]

[22]. Rebuffat A, et al., Comparison of adeno-associated virus pseudotype 1, 2, and 8 vectors administered by intramuscular injection in the treatment of murine phenylketonuria, Hum. Gene Ther 21 (4) (2010) 463–477. [PubMed: 19916803]

[23]. Grisch-Chan HM, et al., Low-dose gene therapy for murine PKU using episomal naked DNA vectors expressing PAH from its endogenous liver promoter, Mol. Ther. Nucleic Acids 7 (2017) 339–349. [PubMed: 28624210]

[24]. Hamman K, et al., Low therapeutic threshold for hepatocyte replacement in murine phenylketonuria, Mol. Ther 12 (2) (2005) 337–344. [PubMed: 16043102]

[25]. Hamman KJ, Winn SR, Harding CO, Hepatocytes from wild-type or heterozygous donors are equally effective in achieving successful therapeutic liver repopulation in murine phenylketonuria (PKU), Mol. Genet. Metab 104 (3) (2011) 235–240. [PubMed: 21917493]

[26]. Harding CO, Gibson KM, Therapeutic liver repopulation for phenylketonuria, J. Inherit. Metab. Dis 33 (6) (2010) 681–687. [PubMed: 20495959]

[27]. Richards DY, et al., AAV-mediated CRISPR/Cas9 gene editing in murine phenylketonuria, Mol. Ther. Methods Clin. Dev 17 (2020) 234–245. [PubMed: 31970201]

[28]. Villiger L, et al., Treatment of a metabolic liver disease by in vivo genome base editing in adult mice, Nat. Med 24 (10) (2018) 1519–1525. [PubMed: 30297904]

[29]. Kaufman S, Max EE, Kang ES, Phenylalanine hydroxylase activity in liver biopsies from hyperphenylalaninemia heterozygotes: Deviation from proportionality with gene dosage, Pediatr. Res 9 (8) (1975) 632–634. [PubMed: 1153238]

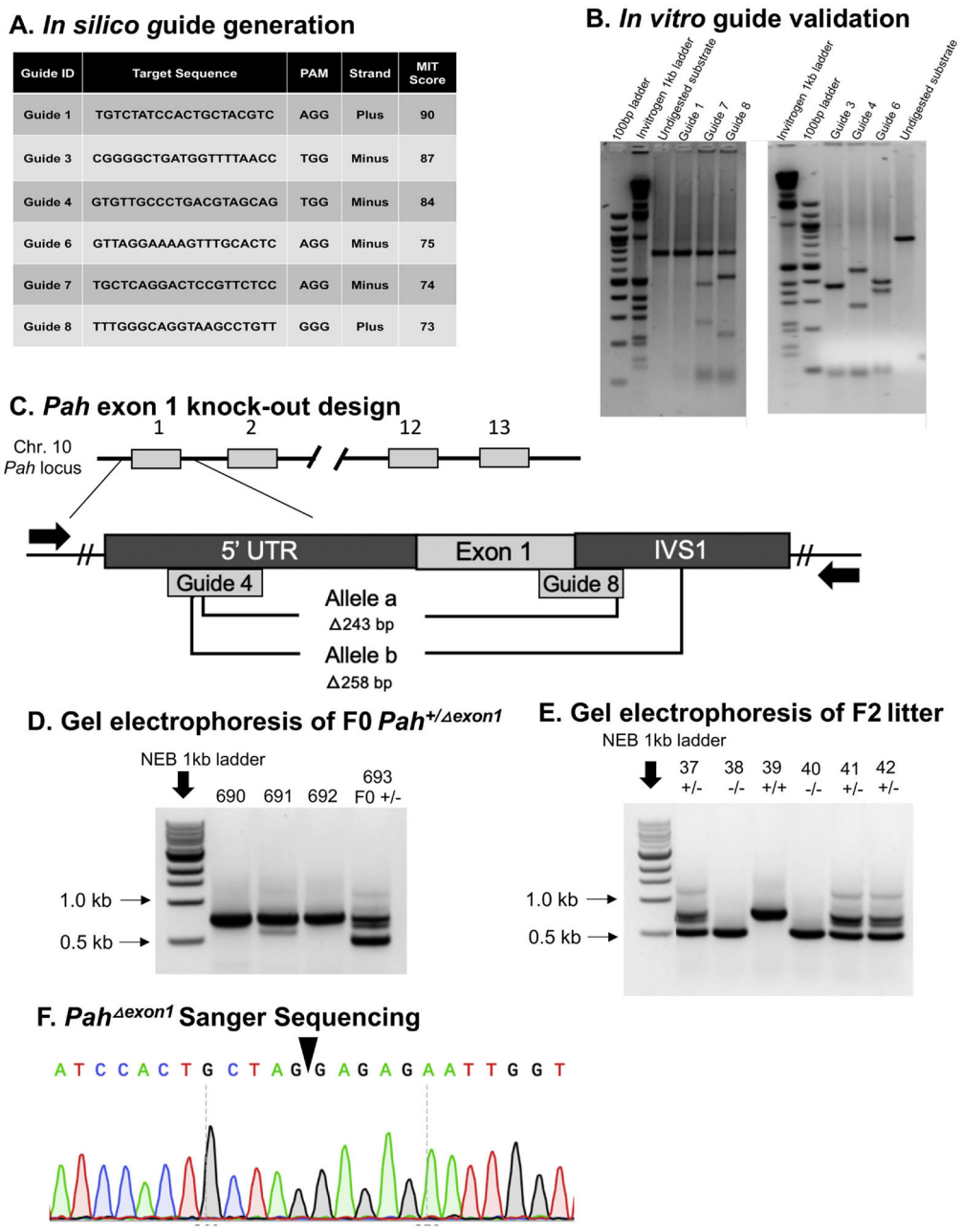

Fig. 1. Experimental design, screening, and sequencing.

A. *In silico* guide generation. The table displays the six guides that were selected for *in vitro* analysis using the MIT Guide Design *in silico* tool. Guide ID, Target Sequence, PAM site, Strand (plus or minus), and MIT Score are displayed, where higher scores indicate an improved prediction for cutting efficiency. B. *In vitro* guide validation. Gel electrophoresis of *in vitro* Guide-It Takara Assay performed with the six guides identified and run on a 3% agarose gel. In the left gel, Guide1 displays no cutting of substrate, while guides 7 and 8 display partial cutting of substrate into 300 bp and 500 bp bands and 200 bp and 600 bp bands, respectively. In the right gel, Guides 3, 4, and 6 show complete cutting of substrate, with a doublet of 400 bp bands from guide 3 cutting, 300 bp and 500 bp from guide 4, and

Guide ID	Target Sequence	PAM	Strand	MIT Score
Guide 1	TGTCTATCCACTGCTACGTC	AGG	Plus	90
Guide 3	CGGGGCTGATGGTTTTAACC	TGG	Minus	87
Guide 4	GTGTTGCCCTGACGTAGCAG	TGG	Minus	84
Guide 6	GTTAGGAAAAGTTTGCACTC	AGG	Minus	75
Guide 7	TGCTCAGGACTCCGTTCTCC	AGG	Minus	74
Guide 8	TTTGGGCAGGTAAGCCTGTT	GGG	Plus	73

350 bp and 450 bp from guide 6. Of note, guide 1 was the only guide that did not demonstrate substrate cutting. C. *Pah* exon 1 knockout design. The diagram illustrates the experimental design to use CRISPR/Cas9 mediated technology with strategically selected sgRNAs to knockout exon 1 of the *Pah* locus. The gene structure of murine *Pah*, located on chromosome 10, is shown with exon 1, exon 2, exon 12, and exon 13 labelled, and // indicates the gene structure containing exons 3–11. Locations of Guide 4 (5′ UTR) and Guide 8 (exon1-IVS1 junction) are displayed and placed below the *Pah* structure due to targeting of the minus strand DNA sequence. The PCR design to detect large, 200+ bp deletions in the 5′ *Pah* locus is indicated with black arrows to represent primers. Forward primer is located in the 5′ UTR and 3′ primer is located in IVS1 (where // indicates DNA gap), resulting in amplification a 753 bp product that flanks exon 1 in the absence of gene modification. Two founder females were identified with deletions spanning exon 1; one animal contained a deletion of 243 bp, designated allele a, and the other animal contained a deletion of 258 bp, designated allele b. D. Gel electrophoresis of F0 $Pah^{+/\Delta exon1}$ female mouse. Tail biopsy DNA from potential $Pah^{+/\Delta exon1}$ founder mice was amplified with the primers described in Fig. 1C. All mice have expected the expected wild type ~750 bp band but founder b (693) carries an additional ~500 bp band representing an allele with a ~ 250 bp deletion. E. Gel electrophoresis of F2 $Pah^{\Delta exon1}$ allele progeny. Genotyping of the progeny from a $Pah^{+/\Delta exon1}$ X $Pah^{+/\Delta exon1}$ breeding: Mouse 37 ($Pah^{+/\Delta exon1}$), Mouse 38 ($Pah^{\Delta exon1/\Delta exon1}$), Mouse 39 ($Pah^{+/+}$), Mouse 40 ($Pah^{\Delta exon1/\Delta exon1}$), Mouse 41 ($Pah^{+/\Delta exon1}$), and Mouse 42 ($Pah^{+/\Delta exon1}$). $Pah^{+/+}$ contains a single ~750 band, $Pah^{+/\Delta exon1}$ contains two bands, a ~ 750 bp band and a ~ 500 bp band, and $Pah^{\Delta exon1/\Delta exon1}$ contains a single ~500 bp band. E. Sanger sequencing of $Pah^{\Delta exon1}$ Allele. The chromatogram displays 12 nucleotides spanning in either direction from the deleted region in the $Pah^{\Delta exon1}$ allele, indicated with the black triangle.

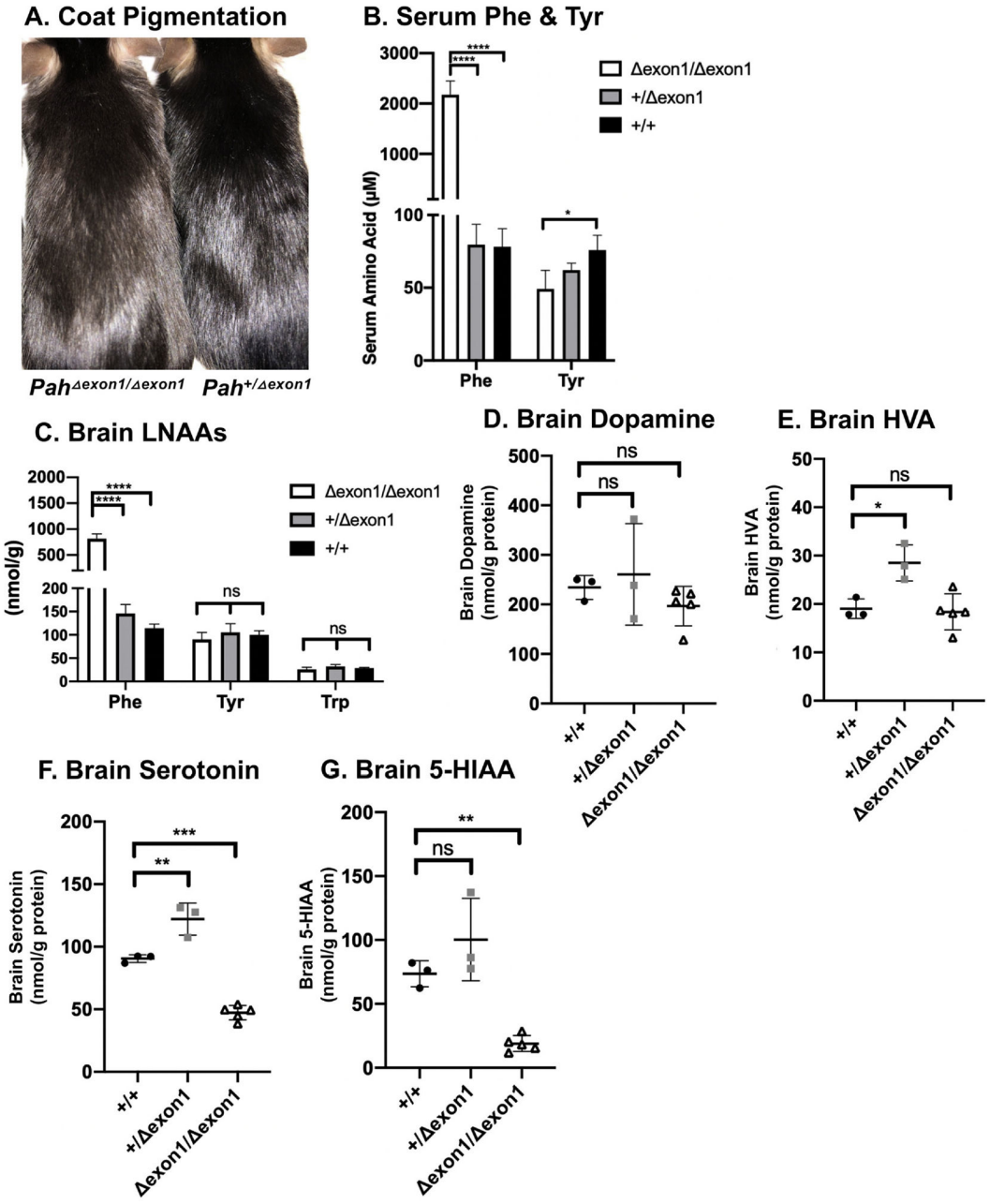

Fig. 2. Characterization amino acids & derivatives in *Pah*$^{\Delta exon1}$ mice.

A. Coat pigmentation. Photograph of untreated *Pah*$^{\Delta exon1/\Delta exon1}$ (left) and *Pah*$^{+/\Delta exon1}$ (right) mice on standard mouse chow diet. B. Serum Phe & Tyr. Mean serum phenylalanine and tyrosine concentration (± SD) of adult *Pah*$^{\Delta exon1/\Delta exon1}$, *Pah*$^{+/\Delta exon1}$, and *Pah*$^{+/+}$ animals following euthanasia. The left y-axis indicates μM serum amino acid concentration. The average serum Phe was 2172 μM, 80 μM, and 78 μM, respectively. One-way ANOVA revealed significant effects of genotype on serum Phe ($F(2,9) = 156.7$, $P < 0.0001$). The average serum Tyr was 49 μM, 62 μM, and 75 μM, respectively. One-way ANOVA revealed significant effects of genotype on serum Tyr between *Pah*$^{\Delta exon1/\Delta exon1}$ and *pah*$^{+/+}$ animals ($F(2, 9) = 6.090$, $P = 0.0213$). C. Brain LNAAs. Mean brain LNAA concentrations (± SD) of

Pah$^{\Delta exon1/\Delta exon1}$, and *Pah*$^{+/+}$ animals at time of euthanasia. The y-axis indicates amino acid concentration in nmol/g wet weight. The average brain Phe was 817 nmol/g, 146 nmol/g, and 114 nmol/g, respectively. One-way ANOVA revealed significant effects of genotype on brain Phe ($F(2, 9) = 154.2$, $P < 0.0001$). The average brain Tyr was 90 nmol/g, 105 nmol/g, and 100 nmol/g, respectively and brain Trp was 26 nmol/g, 32 nmol/g, 28 nmol/g, respectively. One-way ANOVA revealed no statistical differences in brain Tyr or Trp in *Pah*$^{\Delta exon1}$ allele mice. D. Brain dopamine. Brain dopamine concentrations in nmol/g protein (y-axis) of individual animals (represented as single points) in each genotype of *Pah*$^{\Delta exon1}$ allele mice (x-axis). There was no statistical significance in brain dopamine across genotypes by one-way ANOVA ($F (2,8) = 1.129$, $P = 0.3700$). E. Brain HVA. Brain HVA concentrations in nmol/g protein (y-axis) of individual animals (represented as single points) in each genotype of *Pah*$^{\Delta exon1}$ allele mice (x-axis). There was a significant difference in brain HVA across genotypes (one-way ANOVA $F = [2,8] = 9.349$, $p = 0.0081$) with post-hoc multiple comparisons showing a significant increase of HVA in heterozygous animals in comparison to WT animals (adjusted $P = 0.016$) but no difference between homozygous and WT animals (adjusted $P = 0.9453$). F. Brain serotonin in *Pah*$^{\Delta exon1}$ allele mice. Brain serotonin concentrations in nmol/g protein (y-axis) of individual animals (represented as single points) in each genotype of *Pah*$^{\Delta exon1}$ allele mice (x-axis). There was a significant difference in brain serotonin across genotypes (one-way ANOVA ($F [2,8] = 91.20$, $P < 0.0001$), with significantly less brain serotonin in *Pah*$^{\Delta exon1/\Delta exon1}$ animals (47.30 nmol/g protein) than wild type (90.53 nmol/g protein) or heterozygous (122.1 nmol/g protein) animals. G. Brain 5-HIAA. Brain 5-HIAA concentrations in nmol/g protein (y-axis) of individual animals (represented as single points) in each genotype of *Pah*$^{\Delta exon1}$ allele mice (x-axis). There was a significant difference in brain 5-HIAA across genotypes (one-way ANOVA: $F [2,8] = 22.42$, $p = 0.0005$), with less brain 5-HIAA in *Pah*$^{\Delta exon1/\Delta exon1}$ animals (18.95 nmol/g protein) than wild type (73.6 nmol/g protein) or heterozygous (100.3 nmol/g protein) animals.

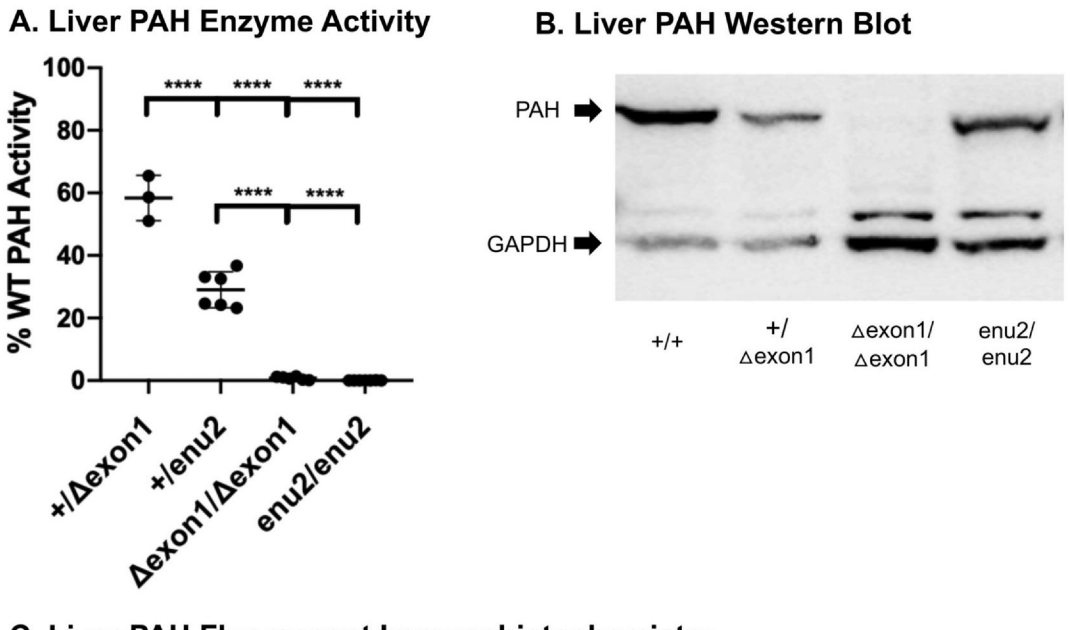

Fig. 3. Characterization of PAH in *Pah*$^{\Delta exon1}$ Mice.

A. Liver PAH enzyme activity. Mean liver PAH enzyme activity (± SD) in homozygous and heterozygous *Pah*$^{\Delta exon1}$ and *Pah*^{enu2} mice. The y-axis indicates liver PAH activity expressed as percent wild type (WT) PAH enzyme activity. The average enzyme activity was 58% in *Pah*$^{+/\Delta exon1}$ and 29% in *Pah*$^{+/\Delta enu2}$, while all homozygous recessive animals were 0%. One-way ANOVA revealed statistical differences in percent WT PAH enzyme activity across these genotypes ($F(3, 18) = 212.7$, $P < 0.0001$). B. Liver PAH Western blot. Western blot analysis of anti-PAH and anti-GAPDH in liver homogenates from *Pah*$^{\Delta exon1}$ allele and *pah*$^{enu2/enu2}$ mice. The arrows on the left of the image indicate band sizes for PAH at 50 kDa (top) and GAPDH at 37 kDa (bottom). C. Liver PAH fluorescent immunohistochemistry. Anti-PAH fluorescent immunohistochemistry in liver tissue samples from *Pah*$^{+/+}$ and *Pah*$^{\Delta exon1/\Delta exon1}$ mice. Green indicates the presence of PAH by anti-PAH antibodies bound by secondary antibodies conjugated with AlexaFluor 488 (green fluorescence) and blue indicates nuclear staining with DAPI. The left image depicts PAH IHC on untreated *Pah*$^{+/+}$ liver tissue with strong green signal and top right image displays PAH IHC of untreated *Pah*$^{\Delta exon1/\Delta exon1}$ liver tissue with absent green signal.

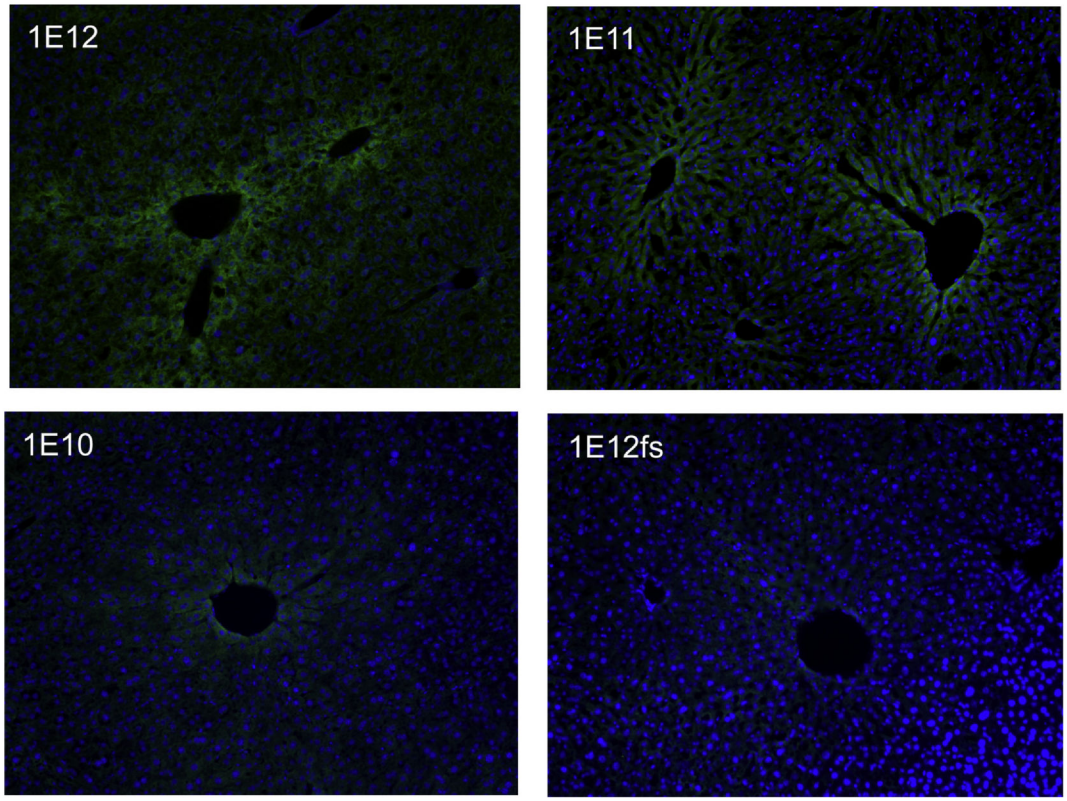

Fig. 4.

Liver PAH Fluorescent Immunohistochemistry of Gene Therapy Treated *Pah*$^{\Delta exon1/\Delta exon1}$ Mice. Anti-PAH fluorescent-immunohistochemistry in liver tissue samples from gene addition therapy treated *Pah*$^{\Delta exon1/\Delta exon1}$ mice. Green indicates the presence of PAH by anti-PAH antibodies bound by secondary antibodies conjugated with AlexaFluor 488 (green fluorescence) and blue indicates nuclear staining with DAPI. The four images display the gene therapy treated *Pah*$^{\Delta exon1/\Delta exon1}$ mice as labelled according to dosing of therapeutic vectors of LSPmPAH AAV2/8: 1×10^{12} vg (top left image labelled with 1E12), 1×10^{11} vg (top right image labelled with 1E11), and 1×10^{10} vg (bottom left image labelled with 1E10), followed by 1×10^{12} vg of the control vector (LSPmPAHfs) containing a frameshift (bottom right image labelled with 1e12fs).

Table 1

Molecular analyses of gene therapy treated *Pah*$^{\Delta exon1/\Delta exon1}$ and *pah*$^{enu2/enu2}$ mice. Pre- and post- gene therapy (GT) effects in a dose escalation experiment in *Pah*$^{\Delta exon1/\Delta exon1}$ mice, as well as gene addition therapy in *pah*$^{enu2/enu2}$ animals. The first column indicates the gene therapy administered, including dose and transgene, where rAAV2/8 LSPmPAH indicates a therapeutic virus containing an rAAV2 genome with a transgene cassette containing a Liver Specific Promoter driving murine PAH packaged into an AAV8 capsid. The AAV2/8 LSPmPAHfs contains a frameshift and is used as a control vector.

Gene therapy	Blood Phe Pre-GT (μM)	Blood Phe Post-GT (μM)	Blood Tyr Pre-GT (μM)	Blood Tyr Post-GT (μM)	Brain Phe Post-GT (μM)	Brain Tyr Post-GT (μM)	Liver PAH activity (%WT)	Vg copy/liver diploid genome
Pah$^{\Delta exon1/\Delta exon1}$ mice								
1E12 AAV2/8 LSPmPAHfs female	2193	1928	38	37	1222	116	0.2%	1.0
1E10 AAV2/8 LSPmPAH male	3095	235	48	117	325	161	4.8%	2.9
1E11 AAV2/8 LSPmPAH female	2677	195	45	115	135	135	42%	16.2
1E12 AAV2/8 LSPmPAH male	1835	127	56	132	382	160	96.1%	50
pah$^{enu2/enu2}$ mice								
1E11 AAV2/8 LSPmPAH 3 male/3 female	1983 ± 540[a]	176 ± 52[a]	ND	ND	ND	ND	7.7 ± 2.2%[a]	8-42[b]
1E12 AAV2/8 LSPmPAH 3 male/3 female	1921 ± 603[a]	99 ± 22[a]	ND	ND	ND	ND	14.8 ± 3.3%[a]	56-291[b]

ND – not done.

[a]Mean ± SD.

[b]Range.